Received: 21 November 2022 | Revised: 27 January 2023 | Accepted: 6 March 2023

DOI: 10.4218/etrij.2022-0426

ORIGINAL ARTICLE

ETRI Journal WILEY

Optimal equivalent-time sampling for periodic complex signals with digital down-conversion

Kyung-Won Kim | **Heon-Kook Kwon** | **Myung-Don Kim**

Terrestrial & Non-Terrestrial Integrated Telecommunications Research Laboratory, Electronics and Telecommunications Research Institute, Daejeon, Republic of Korea

Correspondence
Kyung-Won Kim, Terrestrial & Non-Terrestrial Integrated Telecommunications Research Laboratory, Electronics and Telecommunications Research Institute, Daejeon, Republic of Korea.
Email: kimkw@etri.re.kr

Funding information
This research was supported by the Institute of Information & communications Technology Planning & Evaluation (IITP) grant funded by the Korea government (MSIT; no. 2020-0-00180, "A study for fundamental design and development of 300 GHz channel sounder").

Abstract

Equivalent-time sampling can improve measurement or sensing systems because it enables a broader frequency band and higher delay resolution for periodic signals with lower sampling rates than a Nyquist receiver. Meanwhile, a digital down-conversion (DDC) technique can be implemented using a straightforward radio frequency (RF) circuit. It avoids timing skew and in-phase/quadrature gain imbalance instead of requiring a high-speed analog-to-digital converter to sample an intermediate frequency (IF) signal. Therefore, when equivalent-time sampling and DDC techniques are combined, a significant synergy can be achieved. This study provides a parameter design methodology for optimal equivalent-time sampling using DDC.

KEYWORDS
analog-to-digital conversion, channel sounder, equivalent-time sampling, optimal receiver, periodic signal, radar, ultra-wideband

1 | INTRODUCTION

Mobile traffic is rapidly increasing with various multimedia services; hence, faster wireless communication systems are required. Terahertz and subterahertz frequency bands above 100 GHz are candidates for next-generation communication services owing to their broad bandwidths and favorable propagation characteristics [1]. Studies on propagation and wireless channel characteristics are needed to develop and deploy terahertz services successfully. Various channel sounders have been proposed for wireless channel studies, such as direct sequence spread spectrum (DSSS) [2], orthogonal frequency-division multiplexing (OFDM) [3], chirp signals [4], sliding correlators [5], and frequency-swept vector network analyzers [6]. The vector network analyzer is only suitable for short-range measurements because the cables must connect the transmitter and receiver. Vector network analyzers, sliding correlators, and chirp signal-based sounders have low mobility and are suitable for nontime-varying channel measurements owing to their long measurement durations. OFDM-based channel sounders generally have a lower dynamic range than DSSS-based channel sounders. The DSSS is suitable for channel sounding, providing a high dynamic range and high resolution of the channel impulse response. However, a high-speed analog-to-digital converter (ADC) is required to implement a DSSS-based channel sounder with bandwidths of several gigahertz. We implemented an ultra-wideband channel sounder consisting of a transmitter using

periodic signals and a receiver using **equivalent-time sampling** with **digital down-conversion (DDC)**. This hardware configuration has the advantages of simplicity, inexpensive implementation, and low RF impairment; however, it is limited by the risk of performance degradation due to aliasing. This paper introduces a method to avoid aliasing with the hardware configuration and demonstrates its optimized system performance.

As the bandwidth increases, ensuring a sufficient sampling rate becomes challenging. Nyquist sampling theory provides a minimum sampling rate to avoid aliasing (i.e., Nyquist sampling rate). In low-pass sampling, the Nyquist sampling rate is twice the maximum frequency of the signal [7]. A bandpass (subsampling) receiver can directly receive carrier signals at a sampling frequency lower than twice the maximum frequency [8], thereby reducing the hardware burden and enabling the flexible implementation of a multiband receiver. In bandpass sampling, the Nyquist sampling rate is twice the signal bandwidth [9]. A time-interleaving technique that converts an analog signal into digital data using multiple ADCs and buffers is proposed to implement a high sampling rate. However, as the frequency increases, RF impairment problems (e.g., phase noise, frequency offset, timing skew, and gain imbalance) become severe [10]. In particular, timing skew is problematic in terahertz systems owing to their short wavelengths. Interleaving ADCs [11] and in-phase/quadrature (IQ) sampling [12] are the most common causes of timing skews and gain imbalances as they produce nonlinear impairments [13] that cannot be compensated using deconvolution techniques [14]. System nonlinearity is the most significant cause of spurious multipaths.

Equivalent-time sampling [15] digitizes a periodic signal over multiple periods using a single ADC and a low sampling rate. It can achieve a highly effective sampling rate for periodic signals, and the effective sampling rate increases proportionally with the number of signal repetitions. Equivalent-time sampling avoids the timing skew caused by the interleaved ADC RF parallel structure. However, it carries the risk of aliasing because the sampling rate is lower than the Nyquist rate. The aliasing problems are solved by interpreting nonuniform samples [16]; however, performance degradation is unavoidable in the presence of noise. A DSSS-based channel sounder was proposed in Rey and others [17] using equivalent-time sampling, which avoided aliasing by designing uniformly spaced samples with IQ sampling at the baseband. However, the timing skew and gain imbalance could not be eliminated because the IQ sampling also produced them. A software-defined radio enables DDC rather than analog mixing. Notably, real-valued sampling and DDC are free of IQ imbalances; hence, the use of nonlinear devices can be reduced [18]. An equivalent-time sampling receiver with DDC is free of timing skew and gain imbalance problems owing to its simple RF structure. However, solving the performance degradation caused by aliasing is crucial for combining these two techniques.

The remainder of this paper is organized as follows. Section 2 provides mathematical expressions as preliminary work before finding the optimal system parameters. Section 3 describes the relationship between system parameters and performance based on the signal-to-noise-and-distortion ratio (SNDR). Section 4 introduces our method of finding the optimal system parameters and those that result in irreversible sampling processes. Section 5 presents the measurement results; conclusions are presented in Section 6.

2 | MATHEMATICAL EXPRESSIONS FOR THE EQUIVALENT-TIME SAMPLING OF A CARRIER SIGNAL

Equivalent sampling performs the function of interleaving an ADC over multiple periods with a single ADC. Combining equivalent sampling with DDC simplifies the hardware configuration, solves timing skew and gain imbalance problems, and lowers the required sampling rate. Figure 1A illustrates the structure of an interleaving ADC. Note that equivalent sampling can replace the parallel structure only with a single ADC during multiple periods. Figure 1B,C shows the structures of IQ sampling and DDC-based receivers, respectively. DDC-based equivalent sampling has the simplest structure, and this

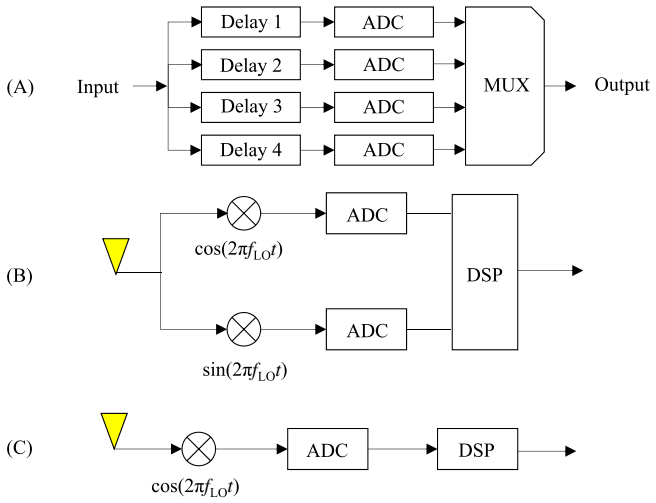

FIGURE 1 Hardware configurations of (A) interleaving analog-to-digital converter (ADC), (B) IQ sampling, and (C) digital down-conversion (DDC)-based equivalent-time sampling.

section discusses its mathematical expressions and carrier signal to derive the optimal system parameter configurations.

A finite number of coefficients can represent a periodic bandlimited signal using a Fourier series:

$$s(t) = \sum_n \alpha_n \cdot \exp\left(j2\pi \cdot \frac{n}{T} \cdot t\right) \tag{1}$$

and

$$N = T \cdot B. \tag{2}$$

$s(\cdot)$, T, B, and t denote the periodic bandlimited baseband signal, period, bandwidth, and time, respectively. α_n and N denote the nth Fourier coefficient and their number, respectively. The frequency response of the periodic bandlimited signal is represented by

$$S(f) = \frac{1}{T} \cdot \sum_n \alpha_n \cdot \delta\left(f - \frac{n}{T}\right), \tag{3}$$

where $S(\cdot)$, $\delta(\cdot)$, and f denote the frequency response, Dirac delta function, and frequency, respectively. A carrier signal with IF is expressed as follows:

$$X(f) = S(f - f_{\mathrm{IF}}), \tag{4}$$

where $X(\cdot)$ and f_{IF} denote the IF signal and the IF, respectively. Equivalent-time sampling collects digital samples of a periodic signal over a longer time than the signal period. A time window is applied to the received signal for acquisition, and the windowed signal can be represented by

$$Y(f) = T_{\mathrm{acq}} \cdot X(f) \otimes \mathrm{sinc}(T_{\mathrm{acq}} \cdot f), \tag{5}$$

where

$$\mathrm{sinc}(\omega) = \begin{cases} \dfrac{\sin(\omega\pi)}{\omega\pi} & \omega \neq 0 \\ 1 & \omega = 0 \end{cases} \tag{6}$$

and

$$T_{\mathrm{acq}} = \frac{M}{f_{\mathrm{s}}}. \tag{7}$$

T_{acq} denotes the acquisition time, M denotes the number of samples received during the acquisition, and f_{s} denotes the sampling rate. The acquisition time is the same as the signal period in Nyquist sampling or interleaving ADC, but it is larger than the signal period of DDC-based equivalent-time sampling.

The DDC system captures only the real part of the IF signal and is expressed by

$$Y_{\mathrm{r}}(f) = \frac{\tilde{S}(f - f_{\mathrm{IF}}) + \widetilde{S^*}(f + f_{\mathrm{IF}})}{2}, \tag{8}$$

where

$$\tilde{S}(f) = T_{\mathrm{acq}} \cdot S(f) \otimes \mathrm{sinc}(T_{\mathrm{acq}} \cdot f) \tag{9}$$

and

$$\widetilde{S^*}(f) = T_{\mathrm{acq}} \cdot S^*(f) \otimes \mathrm{sinc}(T_{\mathrm{acq}} \cdot f). \tag{10}$$

$Y_{\mathrm{r}}(\cdot)$ and $S^*(\cdot)$ denote the frequency responses of the real IF and baseband signals' complex conjugates, respectively. After an analog signal is sampled, the sampling harmonics repeat each sampling rate multiple times. The received signal's discrete fourier transform (DFT) samples are expressed as

$$Y_{\mathrm{s}}[m] = M \cdot \frac{T}{T_{\mathrm{acq}}} \cdot \sum_{i=-\infty}^{\infty} Y_{\mathrm{r}}\left(\frac{m}{T_{\mathrm{acq}}} - i \cdot f_{\mathrm{s}}\right), \tag{11}$$

where $Y_{\mathrm{s}}[m]$ denotes the received signal's mth DFT sample.

Equations (3)–(11) can be expressed by linear equations as follows:

$$y = A \cdot x = \begin{bmatrix} A_1 + A_2 & 0 \\ 0 & A_1 - A_2 \end{bmatrix} \cdot x, \tag{12}$$

where

$$x = \begin{bmatrix} \vdots \\ \mathrm{R}(\alpha_{-1}) \\ \mathrm{R}(\alpha_0) \\ \mathrm{R}(\alpha_1) \\ \vdots \\ \mathrm{I}(\alpha_{-1}) \\ \mathrm{I}(\alpha_0) \\ \mathrm{I}(\alpha_1) \\ \vdots \end{bmatrix}, \quad y = \begin{bmatrix} \vdots \\ \mathrm{R}(Y_{\mathrm{s}}[-1]) \\ \mathrm{R}(Y_{\mathrm{s}}[0]) \\ \mathrm{R}(Y_{\mathrm{s}}[1]) \\ \vdots \\ \mathrm{I}(Y_{\mathrm{s}}[-1]) \\ \mathrm{I}(Y_{\mathrm{s}}[0]) \\ \mathrm{I}(Y_{\mathrm{s}}[1]) \\ \vdots \end{bmatrix}, \tag{13}$$

$$[A_1]_{m,n} = \frac{M \cdot T}{2} \cdot \sum_{i=-\infty}^{\infty} \operatorname{sinc}\left(T_{\text{acq}} \cdot \left(\frac{m}{T_{\text{acq}}} - \frac{n}{T} - f_{\text{IF}} - i \cdot f_{\text{s}}\right)\right), \tag{14}$$

and

$$[A_2]_{m,n} = \frac{M \cdot T}{2} \cdot \sum_{i=-\infty}^{\infty} \operatorname{sinc}\left(-T_{\text{acq}} \cdot \left(\frac{m}{T_{\text{acq}}} + \frac{n}{T} + f_{\text{IF}} + i \cdot f_{\text{s}}\right)\right). \tag{15}$$

A, x, and y denote the sampling matrix, Fourier coefficient vector of the original signal, and received digital sample vector, respectively. $\mathrm{R}(\cdot)$ and $\mathrm{I}(\cdot)$ denote functions that produce outputs as real and imaginary values of the input, respectively. $[\cdot]_{m,n}$ denotes an element of the mth row and nth column of the input matrix.

3 | NOISE AND ERROR ANALYSIS

Theoretically, a received signal can be perfectly reconstructed in an ideal situation using a full-rank sampling matrix. However, the performance of signal reconstruction is limited due to noise. This section analyzes the performance degradation of the equivalent-time receiver with DDC according to random noise. The samples received with noise can be represented by

$$\hat{y} = A \cdot x + w, \tag{16}$$

where w and $\hat{y}$ denote the noise and vector of the received samples with noise, respectively. The noise can be thermal, quantization, phase, or sampling jitter types. Maximum a posteriori estimation is typically used for symbol detection in communication systems. Methods using a priori are not considered because we target random processes, such as a radio channel, in this study. With a white Gaussian noise assumption, maximum likelihood estimation can be achieved using the least-squares method:

$$\hat{x} = A^{+} \cdot \hat{y} = A^{+} \cdot (A \cdot x + w) = x + A^{+} \cdot w, \tag{17}$$

where

$$A^{+} = (A^{\mathrm{T}} \cdot A)^{-1} \cdot A^{\mathrm{T}}. \tag{18}$$

$(\cdot)^{\mathrm{T}}$ denotes a transpose matrix operation, and A^{+} denotes a left-inverse matrix of the sampling matrix. If the sampling matrix is not full-rank, a unique solution cannot be guaranteed by aliasing. Here, when any prior information on the received signal (e.g., channel coding scheme, modulation scheme, or pulse shape) is unknown, the signal reconstruction of a random process in an unknown form is impossible, even without noise. If the number of samples is sufficient, a sampling matrix that is not full-rank cannot be found in IQ sampling because it has twice the number of combinations of A_1 and A_2 in (12). However, when only the in-phase signal is sampled, a nonfull-rank sampling matrix can be obtained, even if the number of samples is sufficient. Figure 2 shows examples of irreversible sampling processes. The left and right columns show the in-phase sampling processes of the different signals. The two signals have the same bandwidth of 3 Hz and the same period of 1 s, but they have different spectra. The first row shows the two signals in the time domain, and the second row shows the Nyquist-sampled spectra. The third and fourth rows show sampling results with a nonfull-rank sampling matrix, which results in aliasing, making reconstruction impossible. Even if the periodic signals are sampled for an infinite time, the two different signals cannot be distinguished by any digital signal processing technique because the sampling results are identical. Thus, setting the appropriate system parameters is crucial for equivalent-time sampling with DDC.

The mean squared error (MSE) of the least-squares solution is computed as

$$\begin{aligned} \varepsilon &= (\hat{x} - x)^{\mathrm{T}} \cdot (\hat{x} - x) \\ &= (A^{+} \cdot w)^{\mathrm{T}} \cdot (A^{+} \cdot w) \\ &= \sum_{n} \left(\sum_{m} [A^{+}]_{n,m} \cdot w_m \right)^2, \end{aligned} \tag{19}$$

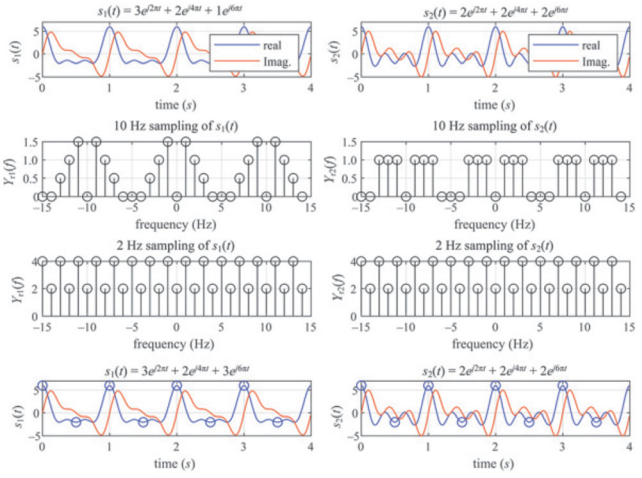

FIGURE 2 Examples of irreversible sampling processes.

where ε and w_m denote the MSE and noise in the mth measurement data, respectively. Therefore, the expected MSE is computed as

$$E[\varepsilon] = \sum_n \left(\sum_m [A^+]_{n,m}^2 \cdot E\left[w_m^2\right] + 2 \cdot \sum_{m_1 \neq m_2} [A^+]_{n,m_1} \cdot [A^+]_{n,m_2} \cdot E[w_{m_1} \cdot w_{m_2}] \right), \tag{20}$$

where $E[\cdot]$ denotes an expectation operation. Assuming w is white Gaussian noise, the following equation is established:

$$E[w_{m_1} \cdot w_{m_2}] = \begin{cases} \frac{P_w}{N} & m_1 = m_2 \\ 0 & m_1 \neq m_2, \end{cases} \tag{21}$$

where P_w denotes noise power within the bandwidth. Therefore, the expected MSE can be computed as

$$E[\varepsilon] = P_w \cdot \|A^+\|_2^2, \tag{22}$$

where

$$\|A^+\|_2 \stackrel{\text{def}}{=} \sqrt{\frac{1}{N} \cdot \sum_n \sum_m [A^+]_{n,m}^2}. \tag{23}$$

As shown in (22), the expected MSE is the product of the noise power and squared matrix norm of the left-inverse matrix. The matrix norm is the degree to which an observation error affects the estimation error in the linear equation, $Ax = y$. The relationship between observation and estimation errors can be represented as

$$\hat{x} - x = A^+ \cdot \hat{y} - A^+ \cdot y = A^+ \cdot (\hat{y} - y). \tag{24}$$

Thus, even a small observation error can result in a large estimation error if the matrix norm is significant.

Figure 3 shows the calculation results of the squared matrix norm based on the IFs. The period is 1.25 ns, and bandwidth is 4 GHz in the calculation. The top-left subfigure shows a case with a 12 GSPS sampling rate. At 12 GSPS, Nyquist sampling can be performed up to a received signal with a maximum frequency of 6 GHz. Because the bandwidth is 4 GHz in the simulation, it corresponds to Nyquist sampling until the IF reaches 4 GHz. The signal reconstruction performance is severely degraded when the IF exceeds 4 GHz and remains less than 8 GHz. However, the top-right subfigure shows a case of equivalent-time sampling with 6 GSPS samplings over two periods. The results differ significantly from the

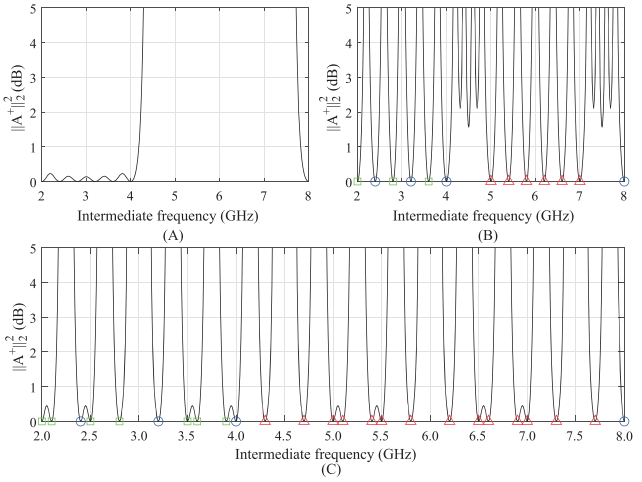

FIGURE 3 Matrix norm calculation results according to an intermediate frequency (IF) when the signal period is 1.25 ns and the bandwidth is 4 GHz: (A) 12 GSPS sampling for one period, (B) 6 GSPS sampling for two periods, (C) 3 GSPS sampling for four periods ($T = 1.25$ ns, $B = 4$ GHz) 2 2.

interpretation of a T-periodic signal or from the bandpass sampling theory. For a carrier signal to be T-periodic, the carrier frequency must be a multiple of 0.8 GHz (=1/1.25 ns). IFs that are T-periodic and are within the Nyquist zone based on the effective sampling rate are represented by blue circles. However, many other optimal IFs can also occur. The optimal IFs that are not T-periodic but are within the Nyquist zone are represented by green squares. Although they are not T-periodic signals, equivalent sampling operates without performance degradation. The optimal IFs that are not T-periodic and are out of the Nyquist zone are represented by red triangles; they do not satisfy the T-periodic signal and Nyquist sampling requirements, but they show optimal performance. The bottom subfigure shows a case of equivalent-time sampling with 3 GSPS samplings over four periods. Even if the IF period is different from the signal period or is outside the Nyquist zone, the performance of many IFs can be same to that of Nyquist sampling under the same SNDR assumptions. However, the matrix norm can diverge to infinity, making reconstruction in the worst case impossible, which in this case is caused by a nonfull-rank sampling matrix.

4 | CONDITIONS FOR OPTIMALITY AND IRREVERSIBILITY

Optimal IFs exist at specific intervals (Figure 3), and clearly, they are related to the signal period. When all the

sinc function inputs in (6) are integers, the sinc function becomes a Dirac delta function. If a sinc function does not become the Dirac delta function owing to a noninteger input, the power spectrum's side lobes have infinite length, and spectral leakage occurs [19]. This result is related to the orthogonality of the received signals and harmonics. The autocorrelation function evaluates the correlation between the original and frequency-shifted signals, and because the autocorrelation function of the sinc function is also a sinc function, two sinc functions are orthogonal only when the interval is a multiple of their widths. Therefore, aliasing caused by spectral leakage is inevitable unless the spacing between all frequencies of the received signal and the sampling harmonics are multiples of $1/T_{\text{acq}}$.

To formulate optimal IFs, we must determine the optimal conditions to avoid spectral leakage. The downconverted DFT samples by DDC can be represented by

$$\begin{aligned} Y_{\text{b}}[m] = & \; M \cdot \frac{T}{T_{\text{acq}}} \cdot \sum_{i=-\infty}^{\infty} Y_{\text{r}}\left(\frac{m}{T_{\text{acq}}} - i \cdot f_{\text{s}} - f_{\text{IF}}\right) \\ = & \; \frac{M \cdot T}{2 \cdot T_{\text{acq}}} \cdot \left(\sum_{i=-\infty}^{\infty} \tilde{S}\left(\frac{m}{T_{\text{acq}}} - i \cdot f_{\text{s}}\right) \right. \\ & \left. + \sum_{i=-\infty}^{\infty} \widetilde{S^*}\left(\frac{m}{T_{\text{acq}}} - i \cdot f_{\text{s}} + 2 \cdot f_{\text{IF}}\right) \right), \end{aligned} \tag{25}$$

where $Y_{\text{b}}[m]$ is the mth downconverted DFT sample. The acquisition time must be a multiple of the period and the IF must be a multiple of $1/(2 \cdot T_{\text{acq}})$ to avoid spectral leakage in (25). Therefore, the following equations are established:

$$T_{\text{acq}} = K \cdot T, \tag{26}$$

$$f_{\text{s}} = \frac{M}{K \cdot T}, \tag{27}$$

and

$$f_{\text{IF}} = \frac{u}{2 \cdot K \cdot T}, \tag{28}$$

where K and u denote the number of periods during the acquisition time and the arbitrary integer used to determine the IF, respectively. By substituting (9), (10), (26), and (28) into (25), (25) can be expressed by

$$\begin{aligned} Y_{\text{b}}[m] = \frac{M \cdot T}{2} \cdot & \sum_{i=-\infty}^{\infty} S\left(\frac{m - i \cdot M}{K \cdot T}\right) \\ & + \sum_{i=-\infty}^{\infty} S^*\left(\frac{m - i \cdot M + u}{K \cdot T}\right) \Bigg). \end{aligned} \tag{29}$$

In equivalent-time sampling, the received signal can be analyzed by reorganizing the collected samples over multiple periods into a single period. A signal representation of the downconverted samples in the time domain is represented by

$$y_{\text{b2}}(t) = \sum_{m=0}^{M-1} y_{\text{b}}[m] \cdot \delta\left(t - m \cdot \frac{K \cdot T}{M}\right), \tag{30}$$

where $y_{\text{b}}[m]$ denotes the mth Inverse DFT sample of $Y_{\text{b}}[\cdot]$ and $y_{\text{b2}}(\cdot)$ denotes the signal representation of the downconverted samples. The signal representation can be divided into multiple single-period signals, as follows:

$$y_{\text{b2}}(t) = \sum_{i=0}^{K-1} y_i(t), \tag{31}$$

where $y_i(\cdot)$ denotes a signal representation of the downconverted signal within the ith period. Therefore, the reorganized signal can be represented as

$$y_{\text{d2}}(t) = \sum_{i=0}^{K-1} y_i(t) \cdot \delta(t + i \cdot T), \tag{32}$$

where $y_{\text{d2}}(\cdot)$ denotes the reorganized signal. The DFT samples of the reorganized signal can be computed as

$$\begin{aligned} Y_{\text{d}}[m] & = \sum_{i=0}^{K-1} Y_i\left(\frac{m}{T}\right) \cdot \exp\left(-j2\pi \cdot \frac{m}{T} \cdot i \cdot T\right) \\ & = \sum_{i=0}^{K-1} Y_i\left(\frac{m}{T}\right) = Y_{\text{b2}}\left(\frac{m}{T}\right), \end{aligned} \tag{33}$$

where $Y_i(\cdot)$ and $Y_{\text{b2}}(\cdot)$ denote the frequency responses of $y_i(\cdot)$ and $y_{\text{b2}}(\cdot)$, respectively. Because $Y_{\text{b}}[\cdot]$ is the DFT of the downconverted samples, (29) can be rewritten as

$$Y_{\text{b}}[m] = Y_{\text{b2}}\left(\frac{m}{K \cdot T}\right). \tag{34}$$

Considering (33) and (34), the DFT of the reorganized samples reflects the downsampled DFT samples of the downconverted samples. Equation (33) can be rewritten as

$$Y_{\text{d}}[m] = Y_{\text{b}}[m \cdot K]. \tag{35}$$

This relationship can be explained by the duality between time and frequency. When an analog signal is sampled or a high-resolution signal is downsampled in the time domain, the harmonics of the high-frequency components enter frequencies below the sampling rate. Similarly, if samples of multiple periods shift to the first

period in the time domain, it is equivalent to downsampling in the frequency domain.

Substituting (29) into (35), (35) can be rewritten as

$$Y_{\mathrm{d}}[m] = S_0[m] + S_1[m] + S_2[m], \tag{36}$$

where

$$S_0[m] = \frac{M \cdot T}{2} \cdot S\left(\frac{m}{T}\right), \tag{37}$$

$$S_1[m] = \frac{M \cdot T}{2} \cdot \sum_{i \neq 0} S\left(\frac{m \cdot K - i \cdot M}{KT}\right), \tag{38}$$

and

$$S_2[m] = \frac{M \cdot T}{2} \cdot \sum_{i} S^*\left(\frac{m}{T} - \frac{i \cdot M - u}{K \cdot T}\right). \tag{39}$$

$S_0[m]$ and $S_1[m]$ denote the mth DFT samples and harmonics of the received signal, respectively. $S_2[m]$ denotes the mth DFT sample of the conjugate signal and its harmonics, respectively.

Only cases in which K and M are coprime are considered to simplify the above equations. As M is the number of samples during K periods, K and M can be parameterized using coprime integers by reducing the fraction. For example, if 2002 samples are taken during four periods, it is equivalent to taking two snapshots of 1001 samples over two periods. When K and M are coprime, this reorganization can be represented by deinterleaving as

$$y_{\mathrm{d}}[m_{\mathrm{d}}] = y_{\mathrm{b}}[m_{\mathrm{b}}], \tag{40}$$

where

$$m_{\mathrm{d}} = \mathrm{rem}(K \cdot m_{\mathrm{b}}, M). \tag{41}$$

$y_{\mathrm{d}}[m]$ denotes the mth deinterleaved sample, and $\mathrm{rem}(p,q)$ denotes the remainder when p is divided by q, where p and q are integers. m_{d} and m_{b} denote the sample indices of the deinterleaved and downconverted data, respectively. A periodic bandlimited signal has nonzero tones only at frequencies of n/T, as explained in (3). When K and M are coprime, $S_1[\cdot]$ has nonzero values only when the i values are multiples of K and can be simplified as

$$S_1[m] = \frac{M \cdot T}{2} \cdot \sum_{i \neq 0} S\left(\frac{m - iM}{T}\right). \tag{42}$$

If only nonzero tones are selected in $S_2[\cdot]$, then (39) is rewritten as

$$S_2[m] = \frac{M \cdot T}{2} \cdot \sum_{i=-\infty}^{\infty} S^*\left(\frac{m}{T} - \frac{i \cdot M - a - b \cdot K}{K \cdot T}\right), \tag{43}$$

where a and b denote the remainder and quotient when u is divided into K. Considering (43), the ith harmonic of the conjugate signal appears at the center frequency of $(i \cdot M - a - b \cdot K)/K \cdot T$. For the ith harmonics to survive after deinterleaving, $(i \cdot M - a - b \cdot K)$ must be a multiple of K. To determine the surviving harmonics after deinterleaving, the following equation is established:

$$a = f(v) = \mathrm{rem}(v \cdot M, K), \tag{44}$$

where v is the minimum positive integer of i, which makes $(i \cdot M - a - b \cdot K)$ a multiple of K. Thus, nonzero frequency components exist only when the i values are $(i \cdot K + v)$ in (43). Substituting $(i \cdot K + v)$ into i in (43), (43) can be rewritten using (44):

$$S_2[m] = \frac{M \cdot T}{2} \cdot \sum_{i=-\infty}^{\infty} S^*\left(\frac{m - i \cdot M}{T} - \frac{f^{-1}(a) \cdot M - a - b \cdot K}{K \cdot T}\right). \tag{45}$$

As shown in (42) and (45), the harmonics repeat every M/T, as do the carrier frequencies that provide orthogonality. Therefore, (28) can be rewritten as

$$f_{\mathrm{IF}} = \frac{a + b \cdot K + c \cdot M \cdot K}{2 \cdot K \cdot T}, \tag{46}$$

where c denotes an arbitrary integer. To be orthogonal between (37) and (45), M/T must be larger than twice the bandwidth:

$$\frac{M}{T} \geq 2 \cdot B = \frac{2 \cdot N}{T}. \tag{47}$$

Equation (47) indicates that the number of received samples must be greater than or equal to twice the number of Fourier coefficients to avoid aliasing. This is equal to the degrees of freedom (DoF) of the original signal. This result is the same as that of the compressed sensing principles [20]. If (47) is satisfied, then (37) and (42) are also orthogonal. The additional inequalities for orthogonality are calculated as follows:

$$\frac{f^{-1}(a) \cdot M - a - b \cdot K}{K \cdot T} \leq -B \tag{48}$$

and

$$B \leq \frac{f^{-1}(a) \cdot M - a - b \cdot K}{K \cdot T} + \frac{M}{T}. \tag{49}$$

Inequalities (48) and (49) represent the conditions in which harmonics are not within the baseband signal bandwidth. They can be merged as

$$N - g(a) \le b \le M - N - g(a), \tag{50}$$

where

$$g(a) = \frac{a - f^{-1}(a) \cdot M}{K}. \tag{51}$$

When (50) is satisfied, only the original signal exists in the bandwidth without harmonics. Therefore, the received signal can be reconstructed using lowpass filtering.

The conditions for optimality can be summarized as follows. At first, the acquisition time is a multiple of the signal period and sampling interval. Secondly, the numbers of received samples and signal period are coprime integers during acquisition. Thirdly, the IF is a multiple of half the inverse of the acquisition time. Fourthly, inequality (50) is satisfied. The optimal IFs in Figure 3 can be calculated using the conditions described in this section. In our simulation, K and M are coprime, and M is greater than twice that of N. The acquisition time and sampling rate are given by (26) and (27), respectively. Because K is two in the top-right subfigure, a is zero or one. Therefore, the range of b for the optimal IFs is given by $5 \le b \le 10$ and $12 \le b \le 17$ for a are zero and one, respectively. If c is set to zero, the optimal IFs are calculated as 2.0, 2.4, 2.8, 3.2, 3.6, and 4 GHz when a is zero and 5.0, 5.4, 5.8, 6.2, 6.6, and 7.0 GHz when a is one. Because K is four in the bottom subfigure, a can be in [0–3], and the ranges of b are given as $5 \le b \le 10$, $16 \le b \le 21$, $12 \le b \le 17$, and $8 \le b \le 13$, respectively. The optimal IFs are calculated by $\{2.0, 2.4, 2.8, 3.2, 3.6, 4.0\}$, $\{6.5, 6.9, 7.3, 7.7, 8.1, 8.5\}$, $\{5.0, 5.4, 5.8, 6.2, 6.6, 7.0\}$ and $\{3.5, 3.9, 4.3, 4.7, 5.1, 5.5\}$ GHz, respectively. The integers, $u(= a + b \cdot K + c \cdot M \cdot K)$, make the matrix norm infinite, apart from the optimal integers given above, and the sampling processes are irreversible. These calculation results are in good agreement with the simulation results.

The proposed technique is similar to OFDM and cyclic prefix (CP) techniques. When transmitting successive OFDM symbols over a multipath channel, a guard time interval between symbols is required to prevent intersymbol interference. Zero-padding can be a solution; however, it causes the signal length to be changed by multipath delays. Otherwise, a CP creates an OFDM signal as a periodic signal and maintains the signal period as the length of the original signal. Therefore, the received signal can be expressed as a circular convolution of the original signal and the multipath channel. This factor is crucial for keeping the time-window size unchanged in the channel estimation.

Similarly, the signal period does not change, even when it passes through a multipath channel in the proposed method. If the signal is periodic, then the basis frequencies are always multiples of $1/T$. Therefore, knowing the precise period of a signal is equivalent to knowing its precise basis frequencies. Generally, equivalent-time sampling, frequency, and phase uncertainties exist when a nonperiodic signal is considered or the exact period is unknown. If the transmitter generates a signal with a predetermined period, the uncertainties disappear. Figure 4 shows examples of T-periodic signals. As can be seen in the first subfigure, if the signal period is a multiple of the sampling interval, there is no phase uncertainty in equivalent-time sampling. In the proposed method, it has already been shown mathematically that there is no phase uncertainty because the complex amplitude includes both amplitude and phase. A non-T-periodic signal produces phase uncertainty; however, it can also be converted into periodic signals by repeating the signal every period. After repeating this process, the basis frequencies become multiples of $1/T$. The second and third subfigures show the effects of repetition. The last subfigure shows that the periodicity does not change, even if a signal passes through a multipath channel.

Figure 5 presents a conceptual diagram of the mechanism used to avoid aliasing with DDC-based equivalent-time sampling in this study. When the basis frequencies are known, the receiver must avoid only the aliasing caused by overlapping or spectral leakages. Because spectral leakage is caused by the window function, it is only necessary to design the sampling rate and number of samples so that the basis frequencies are orthogonal to

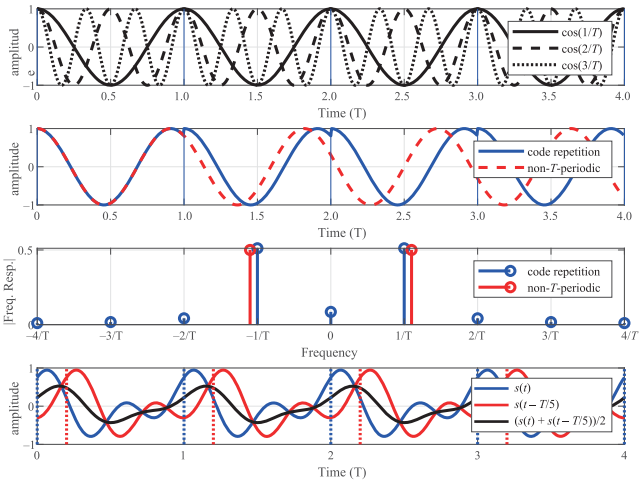

FIGURE 4 Examples of T-periodic and non-T-periodic signals.

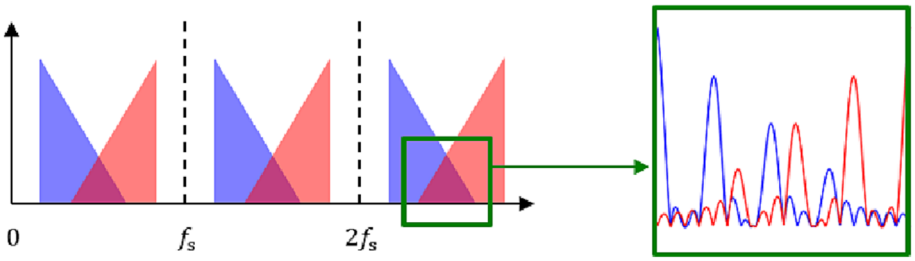

FIGURE 5 Concept diagram of the mechanism used to avoid aliasing during digital down-conversion (DDC)-based equivalent-time sampling.

each other, as explained in this section. Figure 6 shows the optimal system parameters extended in this study using a Venn diagram. The set drawn with a dotted line represents cases in which the received signal and sampling harmonics are orthogonal; hence, the optimal performance can be obtained. The blue set represents cases in which the carrier signal period is the same as that of the baseband signal. The red set indicates cases in which the received signal is in the Nyquist zone, calculated by the effective sample rate. The purple set represents the intersection of the blue and red sets, which are all cases of orthogonal harmonics.

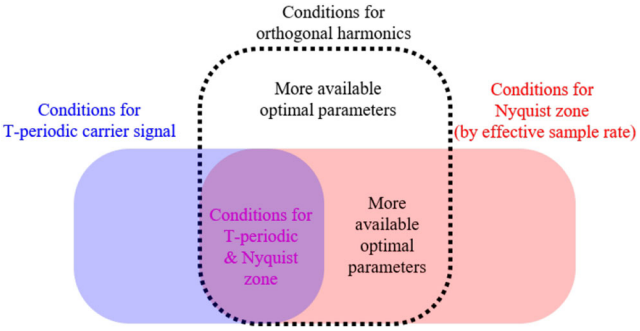

FIGURE 6 Expansion of optimal system parameters for digital down-conversion (DDC)-based equivalent-time sampling by orthogonal harmonics.

5 | MEASUREMENT RESULTS

This section presents the measurement results for two purposes. The first is to verify the optimal parameter conditions introduced in the previous section, and the second is to demonstrate the performance in a real environment with clock drift. Sampling at accurate frequencies and timing is crucial for DDC-based equivalent-time sampling. Sampling jitter can be divided into independent random and accumulated types. The additive white Gaussian noise assumption can be applied to independent sampling jitter, which has a white spectrum and increases the random noise [21, 22] even during equivalent-time sampling [23]. The effect of random noise on this technique is explained in Section 3. However, the accumulated sampling jitter differs from that of random noise. The slip rate (i.e., clock drift velocity) can linearly approximate the accumulated sampling jitter in a short period. This can be interpreted as an offset of the IF and sampling frequency. It is not a problem in wired transceiver systems because the same clock source provides reference signals for both the transmitter and receiver. However, if different clock sources are used in wireless transceiver systems, various frequency offsets may occur and degrade system performance.

The first experiment evaluated the availability of the reconstruction technique using DDC and deinterleaving when the signal was not T-periodic and not within the Nyquist zone. A pseudo noise (PN) sequence was used as the probing signal, where the code length, period, bandwidth, and carrier frequency were 4095, 10.2375 μs, 400 MHz, and 420 MHz, respectively. The signal was sampled at an 88 MSPS sample rate for 102.375 μs. System parameters N, M, K, a, b, and c were set as 4095, 9009, 10, 5, 8599, and 0, respectively. The effective sample rate is 880 MSPS, and the signal generator and oscilloscope were synchronized using a reference cable. Figure 7 shows the measurement and signal reconstruction results. Based on the effective sample rate and Nyquist theory, the IF should be within 200 MHz–240 MHz or 640 MHz–680 MHz. In this case, the IF was out of range, and its period differed from the baseband signal period. However, all conditions for the orthogonal harmonics were satisfied. A mirror image should be centered at 460 MHz based on Nyquist theory after being converted to 40 MHz and repeatedly appearing every 880 MHz. The harmonics were removed during deinterleaving, and the other sampling harmonics were observed with a center frequency of –400 MHz. The observed harmonics were generated by the actual sample rate, not the effective rate, and survived after deinterleaving. As anticipated in Section 4, different results were obtained than those interpreted by effective sampling harmonics and Nyquist theory. Additionally, no aliasing was observed between the received signal and harmonics.

The second measurement test evaluated the accuracy of the actual subterahertz band when clock drift existed.

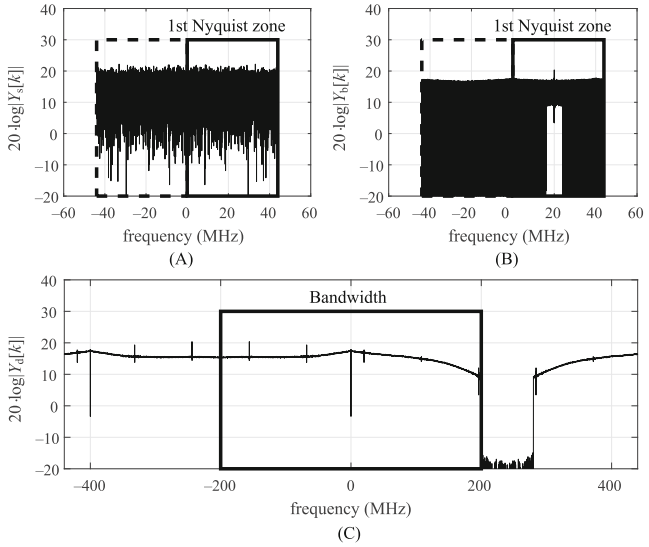

FIGURE 7 Measurement and signal reconstruction results, where the carrier signal is not T-periodic and out of the Nyquist zone: (A) received samples, (B) down-converted samples, (C) deinterleaved samples.

The clock drift between the two asynchronous rubidium oscillators was measured, and the slip rate was approximately 236.8758 ps/s. The PN signal's code length, symbol rate, signal period, and bandwidth were 4095, 4 GHz, 1.02375 μs, and 5 GHz, respectively. The PN signal was generated at the baseband, upconverted to 159 GHz through a 15 GHz IF, and transmitted. After receiving the signal, it was downconverted to 4 GHz through a 15-GHz IF and sampled by 10 GSPS. The clock source error produced offsets at all frequencies, including the IF, carrier frequency, and sampling rate. The frequency offset can be calculated as

$$f_{\text{offset}} = f \cdot \frac{R_{\text{slip}}}{1 + R_{\text{slip}}}, \tag{52}$$

where f_{offset} and R_{slip} denote frequency offset and slip rate, respectively. Therefore, in the experimental environment, the frequency offsets at 4 GHz, 10 GHz, 15 GHz, and 159 GHz were 0.9475 Hz, 2.3688 Hz, 3.5531 Hz, and 37.6633 Hz, respectively. The proposed sampling method was performed using three ways. The first dataset was sampled for two periods, the second was downsampled eight times after being sampled over 16 periods, and the third was downsampled 4096 times after being sampled over 8192 periods. The effective sample rate was 20 GSPS, whereas the actual sample rates were 10, 1.25, and 10/4096 GSPS ($\approx$2.4414 MSPS). Then, the power delay profiles were calculated by correlating them with the original PN signal after applying a system response deconvolution and raised cosine (RC) filter. The 3-dB

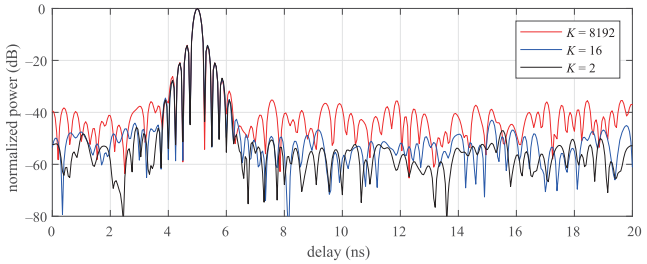

FIGURE 8 Measurement results of power delay profiles according to the number of signal repetitions under the same number of samples. The sample rate is inversely proportional to the number of repetitions.

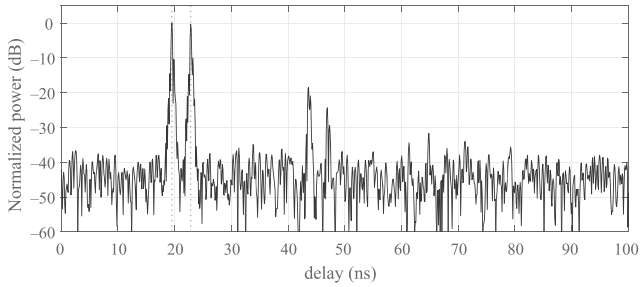

FIGURE 9 Measurement results of power delay profiles with two reflectors at 3 m and 3.5 m from the antennas.

bandwidth and roll-off factors of the RC filter were 4 GHz and 1.25, respectively. Figure 8 shows the results of power delay profile measurements. The number of received samples was 20475 in all cases. Consequently, the longer the acquisition time after the holdover, the worse was the performance owing to clock drift at the same slip rate. Even in an asynchronous environment, measuring a dynamic range of approximately 40 dB with 2.4414-MSPS sampling of a 5-GHz bandwidth signal was possible. Figure 9 shows the measurement results in air using the same hardware configuration. The transmitter and receiver faced two reflectors placed at 3.0 m and 3.5 m distances, respectively. Both sides of the reflector were blocked with absorbers. Horn antennas with a 10 degree beamwidth were used as the transmitter and receiver. Multipath delays of 20 ns and 23.3333 ns were observed, which equaled the round-trip distance between antennas and reflectors. The red dotted line represents the calculated delays. Multipaths that hit the channel sounder body and traveled twice between the channel sounder and reflectors were also observed between 40 and 50 ns.

6 | CONCLUSIONS

This study introduced a system design method with equivalent-time sampling and DDC that avoids aliasing.

The proposed technique can be applied to channel sounders and measurement systems for radar, biomedical sensing, and imaging requirements. If a probing signal can be repeated, it can be used for any application. A receiver can thus be implemented using a low-cost, low-power, lightweight, small, and flexible device because its hardware configuration can be simplified, and digital processing techniques can replace the hardware.

CONFLICT OF INTEREST STATEMENT

The authors declare that there are no conflicts of interest.

ORCID

Kyung-Won Kim https://orcid.org/0000-0002-9663-9954

REFERENCES

1. T. S. Rappaport, Y. Xing, O. Kanhere, S. Ju, A. Madanayake, S. Mandal, A. Alkhateeb, and G. C. Trichopoulos, *Wireless communications and applications above 100 GHz: opportunities and challenges for 6G and beyond*, IEEE Access **7** (2019), 78729–78757.
2. R. Zhang, S. Wang, X. Lu, W. Duan, and L. Cai, *Two-dimensional DoA estimation for multipath propagation characterization using the array response of PN-sequences*, IEEE Trans. Wireless Commun. **15** (2016), no. 1, 341–356.
3. Y. Samayoa, M. Kock, H. Blume, and J. Ostermann, *Low-cost channel sounder design based on software-defined radio and OFDM*, (Proc. IEEE 88th Vehicul. Technol. Conf. (VTC-Fall), Chicago, IL, USA), 2018, pp. 27–30.
4. N. Hosseini and D. W. Matolak, *Wide band channel characterization for low altitude unmanned aerial system communication using software defined radios*, (Proc. ICNS Conf., Herndon, VA, USA), 2018, pp. 10–12.
5. G. R. Jr, T. S. MacCartney, and A Rappaport, *Flexible millimeter-wave channel sounder with absolute timing*, IEEE J. Select. Areas Commun. **35** (2017), no. 6, 1402–1418.
6. Y. Ji, W. Fan, and G. F. Pedersen, *Channel characterization for wideband large-scale antenna systems based on a low-complexity maximum likelihood estimator*, IEEE Trans. Wireless Commun. **17** (2018), no. 9, 6018–6028.
7. C. E. Shannon, *Communication in the presence of noise*, Proc. IRE **37** (1949), no. 1, 10–21.
8. M. Brandolini, P. Rossi, D. Manstretta, and F. Svelto, *Toward multistandard mobile terminals—fully integrated receivers requirements and architectures*, IEEE Trans. Microwave Theory Techniq. **53** (2006), no. 3, 1026–1038.
9. R. G. Vaughan, N. L. Scott, and D. R. White, *The theory of bandpass sampling*, IEEE Trans. Signal Process. **39** (1991), no. 9, 1973–1984.
10. A. Mohammadian and C. Tellambura, *RF impairments in wireless transceivers: phase noise, CFO, and IQ imbalance—a survey*, IEEE Access **9** (2021), 111718–111791.
11. C. Vogel, *The impact of combined channel mismatch effects in time-interleaved ADCs*, IEEE Trans. Instrum. Meas. **54** (2005), no. 1, 415–427.
12. Y. R. Ramadan, H. Minn, and M. E. Abdelgelil, *Precompensation and system parameters estimation for low-cost nonlinear tera-hertz transmitters in the presence of I/Q imbalance*, IEEE Access **6** (2018), 51814–51833.
13. H. Cao, A. S. Tehrani, C. Fager, T. Eriksson, and H. Zirath, *I/Q imbalance compensation using a nonlinear modeling approach*, IEEE Trans. Microwav. Theor. Techniq. **57** (2009), no. 3, 513–518.
14. R. Sun, P. B. Papazian, J. Senic, Y. Lo, J.-K. Choi, K. A. Remley, and C. Centile, *Design and calibration of a double-directional 60 GHz channel sounder for multipath component tracking*, (Proc. 11th EuCAP, Paris, France), 2017, pp. 19–24.
15. Z. Zhu, Y. Zhu, D. Li, and M. Liu, *A TD-ADC for IR-UWB radars with equivalent sampling technology and 8-GS/s effective sampling rate*, IEEE Trans. Circuit. Sys. II **68** (2021), no. 3, 888–892.
16. Y.-P. Lin and P. P. Vaidyanathan, *Periodically nonuniform sampling of bandpass signals*, IEEE Trans. Circuit Sys. II Analog Digit. Sig. Process. **45** (1998), no. 3, 340–351.
17. S. Rey, J. M. Eckhardt, B. Peng, K. Guan, and T. Kurner, *Channel sounding techniques for applications in THz communications—a first correlation based channel sounder for ultra-wideband dynamic channel measurements at 300 GHz*, (Proc. 9th ICUMT, Munich, Germany), 2017, pp. 6–8.
18. G. Fettweis, M. Lohning, D. Petrovic, M. Windisch, P. Zillmann, and W. Rave, *Dirty RF: a new paradigm*, (Proc. IEEE 16th Int. Symp. Person. Indoor Mobile Radio Commun., Berlin, Germany), 2005, pp. 11–14.
19. F. J. Harris, *On the use of windows for harmonic analysis with the discrete Fourier transform*, Proc. IEEE, **66** (1978), no. 1, 51–83.
20. D. L. Donoho, *Compressed sensing*, IEEE Trans. Informat. Theory **52** (2006), no. 4, 1289–1306.
21. Y. C. Jenq, *Digital spectra of nonuniformly sampled signals: fundamentals and high-speed waveform digitizers*, IEEE Trans. Instrum. Meas. **37** (1998), 245–251.
22. S. S. Awad and M. F. Wagdy, *More on jitter effects on sinewave measurements*, IEEE Trans. Instrum. Meas. **40** (1991), 549–552.
23. K. Takahashi, R. Roberts, Z. Jiang, and B. Memarzadeh, *Statistical evaluation of signal-to-noise ratio and timing jitter in equivalent-time sampling signals*, IEEE Trans. Instrum. Meas. **70** (2021), 1–4.

How to cite this article: K.-W. Kim, H.-K. Kwon, and M.-D. Kim, *Optimal equivalent-time sampling for periodic complex signals with digital down-conversion*, ETRI Journal **46** (2024), 238–249. DOI 10.4218/etrij.2022-0426

AUTHOR BIOGRAPHIES

Kyung-Won Kim received his BS degree in Electrical Engineering from Korea University in Seoul, Republic of Korea, in 2009, and his Ph.D. in Computer and Radio Communications Engineering from Korea University, Seoul, Republic of Korea

in 2015. Since 2015, he has been with ETRI in Daejeon, Republic of Korea, where he is currently a senior researcher. His fields of interest include signal processing, channel estimation, channel modeling, and radio resource management.

Heon-Kook Kwon received his BS and MS degrees at the Department of Electronics Engineering at Chungnam National University in Daejeon, Republic of Korea, in 1997 and 1999, respectively. He joined ETRI in Daejeon, Republic of Korea in 2004. As a principal researcher, he worked on developing RF systems for mobile communications, including those of mobile and base stations. His research interests include RF system design for next-generation mobile communications.

Myung-Don Kim received his BS and MS degrees in Electronics Engineering from Dong-A University in Busan, Republic of Korea, in 1993 and 1995, respectively. Since 1995, he has been with ETRI, Daejeon, Republic of Korea, where he is a principal researcher at the Telecommunications and Media Research Laboratory. He was the Director of the Mobile RF Research Section from 2017 to 2018 and is currently a project leader in the Channel Modeling Research Group. His research interests include wireless channel measurements and modeling. Since 2006, he has been involved in many projects developing wideband MIMO channel sounders, field measurements, and channel models. He contributed to the development of ITU-R recommendations and reports in Study Group 3 (Propagation), including millimeter-wave propagation models. Since 2014, he has been the chairperson of the ITU-R WP3K Draft Group 3K-3A, which studies prediction methods for short-path outdoor propagations in frequencies from 300 to 100 GHz.